2294–2303 *Nucleic Acids Research, 2011, Vol. 39, No. 6* *Published online 18 November 2010*
doi:10.1093/nar/gkq800

Single-Molecule characterization of oligomerization kinetics and equilibria of the tumor suppressor p53

Sridharan Rajagopalan[1], Fang Huang[1,2,*] and Alan R. Fersht[1,*]

[1]MRC Centre for Protein Engineering, Hills Road, Cambridge, CB2 0QH, UK and [2]Center for Bioengineering and Biotechnology, China University of Petroleum, Qingdao, Shandong, 266555, China

Received June 10, 2010; Revised August 9, 2010; Accepted August 27, 2010

ABSTRACT

The state of oligomerization of the tumor suppressor p53 is an important factor in its various biological functions. It has a well-defined tetramerization domain, and the protein exists as monomers, dimers and tetramers in equilibrium. The dissociation constants between oligomeric forms are so low that they are at the limits of measurement by conventional methods *in vitro*. Here, we have used the high sensitivity of single-molecule methods to measure the equilibria and kinetics of oligomerization of full-length p53 and its isolated tetramerization domain, p53tet, at physiological temperature, pH and ionic strength using fluorescence correlation spectroscopy (FCS) *in vitro*. The dissociation constant at 37°C for tetramers dissociating into dimers for full-length p53 was 50 ± 7 nM, and the corresponding value for dimers into monomers was 0.55 ± 0.08 nM. The half-lives for the two processes were 20 and 50 min, respectively. The equivalent quantities for p53tet were 150 ± 10 nM, 1.0 ± 0.14 nM, 2.5 ± 0.4 min and 13 ± 2 min. The data suggest that unligated p53 in unstressed cells should be predominantly dimeric. Single-molecule FCS is a useful procedure for measuring dissociation equilibria, kinetics and aggregation at extreme sensitivity.

INTRODUCTION

Tumor suppressor p53 decides the fate of cells via transcriptional activation of genes involved in cell-cycle arrest, apoptosis and DNA repair (1). The quaternary structure of p53 is composed of both folded and disordered domains: N-terminal transactivation domain (TAD) which is intrinsically disordered, folded DNA binding core domain (CD), structured tetramerization domain (Tet) and C-terminal negative regulatory domain (CTD) (Figure 1A) (2). p53 is mutated in ~50% of cancers, and the DNA-binding domain is the main carrier of oncogenic mutations (3). Cancerous mutants retain their ability to form tetramers. Hybrid formation between the wild-type (WT) and mutant protein is proposed as the cause for *trans*-dominant effect (gain of mutant function) of the mutant over WT in heterozygous cells (4). The importance of the oligomerization domain to p53′s function is evidenced by mutations in this domain identified in patients with Li-Fraumeni syndrome (5).

Oligomerization plays an important role in p53 activation. Tetrameric p53 binds to its DNA response elements (RE) 100-times more tightly than monomeric core domain (6). Consequently, tetrameric p53 is required for transactivation of p53 target genes (6–9). Moreover, post-translational modifications such as phosphorylation, acetylation and ubiquitination sometimes require p53 to be tetramerized (10–12). Experimentally, formation of tetrameric p53 occurs by the following equilibrium $4M \leftrightarrow 2D \leftrightarrow T$ (where M = monomer, D = dimer and T = tetramer) (13). Furthermore, p53 dimerizes on co-translation in polysomes but tetramerization occurs post-translationally in solution (4).

The dissociation constants between monomer and dimer, and dimer and tetramer are so low that they are difficult to be measured accurately. Previous measurements using analytical ultracentrifugation have been revised to lower values with increasing sensitivity of detectors (14). Furthermore, it has been recently found that the equilibration is very slow (15). Here, we utilized single-molecule fluorescence correlation spectroscopy (FCS), which has the necessary sensitivity to measure the $D \leftrightarrow M$ and $T \leftrightarrow D$ equilibrium of p53 tetramerization domain (p53tet: 325–355) in isolation and in full-length p53 (flp53: 1–393) at 37°C. We provide a quantitative analysis of the thermodynamics and kinetics of oligomerization equilibria of p53. The influence of bax and p21

*To whom correspondence should be addressed. Tel/Fax: +86 532 86981560; Email: fhuang@upc.edu.cn
Correspondence may also be addressed to Alan R. Fersht. Tel: +44 1223 402137; Fax: +44 1223 402140; Email: arf25@cam.ac.uk
Present address:
Sridharan Rajagopalan, Department of Biochemistry, University of Washington, Seattle, WA98195, USA.

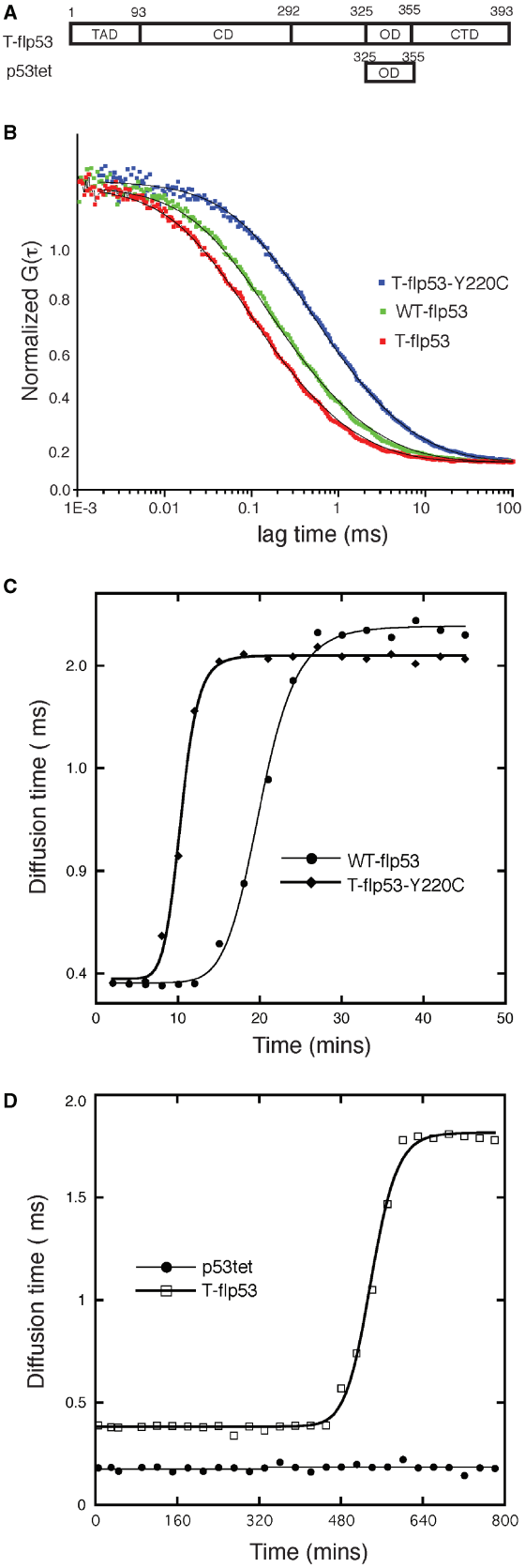

Figure 1. Kinetic stability of p53 studied using FCS. (**A**) Linear representation of p53 domain organization. (**B**) ACFs of WT-flp53, T-flp53 and T-flp53-Y220C measured after 15 min. (**C**) Aggregation kinetics of WT-flp53 and T-flp53-Y220C. (**D**) Aggregation kinetics of super-stable mutant T-flp53 and p53tet.

response elements (REs) in perturbing the D↔T equilibrium was also investigated.

Accurate values on the kinetics and equilibrium constants of p53 oligomerization are not available in literature, which are essential for the understanding of the p53 status in normal and tumor cells and how p53 carries out its functions.

MATERIALS AND METHODS

Materials

Double stranded p21 and bax oligonucleotides labeled with Atto 655 5′-CGCGAACATGTCCCAACATGTTG CGC-3′ and 5′-CGCTCACAAGTTAGAGACAA-GCTT CGC-3′ at 5′ end were purified by high-pressure liquid chromotagraphy (HPLC).

Protein expression, purification and labeling

flp53 was expressed and purified as described (16,17). Peptides corresponding to residues 325–355 of the tetramerization domain for the WT, dimeric (L344A) and monomeric (L344P) carrying an N-terminal cystiene were purchased from Designer Bioscience Ltd, UK (>98% HPLC grade purity). Peptides were labeled with 8-fold excess of Atto-655 maleimide (AD 655-45, ATTO-TEC, Germany) in a buffer containing 20 mM Na_2HPO_4/NaH_2PO_4, 100 mM NaCl, 3 mM TCEP, pH 7.0. Labeling reaction was followed by mass spectrometry. About 90% of the peptide was labeled by 6 h. The mixture was loaded onto a G-25 desalting column to separate residual dye. The peptide fraction collected was loaded onto C-8 column and purified by high-pressure liquid chromatography using water-acetonitrile gradient to separate unlabeled peptide. Atto 655-labeled peptide fractions were collected and freeze-dried. The peptides were dissolved in buffer containing 20 mM Na_2HPO_4/NaH_2PO_4, 150 mM NaCl, 3 mM DTT, pH 7.4 for future experiments. flp53 was labeled using Atto-655 succinimidyl ester and purified as described earlier (18).

FCS experiments

FCS experiments were carried out on a home-built dual-channel confocal fluorescence microscope set-up (Nikon Eclipse TE2000-U). Samples were excited using a Helium-Neon laser at 633 nM, with 100 μW at the back aperture of the microscope lens adjusted using neutral density filter. Fluorescence was collected using an oil-immersion objective (Nikon CFIplan Apochromat VC 100×, numerical aperture 1.4; Nikon), and optically filtered using a dichroic mirror (Semrock, Brightline, FF495/540/650) and a long-pass filter (Semrock, Razor Edge, 647 nm). A pinhole size of 150 μm was used to remove out-of-plane fluorescence photons. The collected fluorescence light was focused onto an avalanche photon counting module (SPCM-AQR15; PerkinElmer). The output from the detector was recorded using a digital hardware correlator (Flex02-01D/C; Correlator.com). Temperature was controlled using a custom-built objective-type heater/cooler. Samples were measured on

Lab-Tek chambered coverglass (Nalge-Nunc, IL, USA) with eight wells. Use of Protein blocker (Block Ace, Snow Brand, Japan) significantly reduced the non-specific adsorption of proteins on the surface of chamber. Measurements were made in physiological ionic strength buffer containing 20 mM Na_2HPO_4/NaH_2PO_4, pH 7.4, 150 mM NaCl, 3 mM DTT. 0.05% Tween-20 and 0.3 mg/ml BSA were used as solvent additives to further suppress glass surface adsorption. In FCS experiments to determine p53 aggregation kinetics, the total concentration of protein was 2 μM (labeled protein concentration of 0.1 nM). For binding experiments, 0.1 nM labeled protein was incubated with increasing amount of unlabeled protein up to a final concentration of 2 μM. Background measurements gave a weak fluorescent count rate of <10 Hz, while the dye-labeled molecules gave an average count rate of 5 KHz. The duration of each measurement was 180 s and each point on the titration curve is represented by average of three independent FCS measurements.

FCS data analysis

FCS measures fluorescence intensity fluctuations within femtoliter detection volumes and a temporal range from nanoseconds to seconds. Fluorescence fluctuations arising from single molecules diffusing through the detection volume in FCS experiments were analyzed via the second order autocorrelation function [G(τ)]:

$$G(\tau) = \frac{\langle I(t)I(t+\tau)\rangle}{\langle I(t)\rangle^2}$$

where I(t) is the fluorescence intensity at time t, I(t + τ) is the fluorescence intensity after a time lag τ, and < > denotes the time average over the total observation time (19,20). Data were fitted to an analytical model containing a single 2D diffusion term described by

$$G(\tau) = \frac{1}{N}\left(\frac{1}{1+\tau/\tau_D}\right)$$

where N is average number of fluorescent molecules in the detection volume, τ is the lag time and τ_D is the experimental diffusion time in two (x,y) dimensions. A 2D model is of sufficient accuracy where the Z-dimension is much larger than x/y, which was the case in the experimental set-up used here.

Two independent diffusion species were modeled using:

$$G(\tau) = \frac{1}{N}\left(\frac{1-y}{1+\tau/\tau_1} + \frac{y}{1+\tau/\tau_2}\right)$$

where τ_1 and τ_2 are the diffusion times of free protein and bound complex, y is the amount (mole fraction) of bound complex. Ensemble measurements confirmed that the fluorescence intensity and hence the molecular brightness did not change during any of the binding events. The least square fit used is based on the Levenberg-Marquardt algorithm in Origin 7.0 (OriginLab).

Binding and rate data analysis

Binding data for $[p53]+[p^*] \leftrightarrow [p^*p53]$ were analyzed with simple binding model based on a 1:1 stochiometry for the bimolecular reaction, where p* represents Atto 655 labeled peptide and p53 represents flp53, using the equation:

$$F_b = \frac{m^*[p53]}{K_d+[p53]} + c$$

where F_b is the fraction of p* bound, m and c are scaling factors, K_d is the dissociation constant. The following Kinetic data were fitted to two sequential first-order processes for $[p53]_4 \rightarrow [p53]_2 \rightarrow [p53]$, since the change in equilibrium on dilution was close to irreversible at the final concentration. Data analysis and curve fitting were performed using Kaleidagraph 4.0.

RESULTS

Determination of stability of p53 with respect to aggregation using FCS

FCS is a method based on fluctuation analysis of fluorescence intensity to characterize time-dependent properties of individual molecules (21). FCS has been extensively used to study protein–protein interactions, protein–ligand binding and large-scale drug screening and more recently for the study of denatured state dynamics of small proteins (19,22–25). FCS analysis directly provides the average number of fluorescent molecules in the observation volume and the translational diffusion time of molecules. The latter is proportional to the solution viscosity and the hydrodynamic radius. The binding or interaction of proteins can be effectively detected with FCS due to the third root dependence of hydrodynamic radius on molecular weight (26).

In contrast to many ensemble techniques, the presence of even a small amount of aggregates in the sample material is signaled by species of very slow diffusion times, typically of the order of a few milliseconds in the apparatus used. WT p53 is highly unstable with a T_m of 44°C, with reversible denaturation being followed by fast irreversible aggregation (27). We first measured the kinetic stability (time-dependent aggregation) of flp53 and p53tet in order to avoid any aggregation in the course of experiments. We assessed in real-time the rate of aggregate formation of three different forms of flp53: WT (WT-flp53), a super-stable quadruple mutant (T-flp53) (28) and a destabilized mutant Y220C in the super-stable mutant background (T-flp53-Y220C) (Figure 1B). T-flp53 carries four mutations (M133LV203AN239YN268D), stabilizing p53 by 2.65 kcal mol^{-1} and increasing its T_m by 5.6°C (28). The mutant protein T-flp53-Y220C, with an additional highly destabilizing Y220C mutation (29), was used as a further control. Proteins were labeled at the amino terminus using the extrinsic fluorophore Atto 655. This label is advantageous for FCS studies because of its insignificant triplet formation rate, limiting the number of parameters of fit thereby making the analysis of

autocorrelation data robust and reliable (30). Autocorrelation functions (ACF) were measured for different time intervals and the diffusion times were obtained by fitting the ACFs to single component 2D diffusion model. Single-component fits of ACFs for samples with aggregates showed slight deviations in residuals, which is probably due to the heterogeneous nature of aggregates. Aggregation of T-flp53-Y220C and WT-flp53 was observed as early as 5 and 20 min, respectively, after raising the temperature to 37°C, from the appearance of slowly diffusing species with diffusion time of ~2.1 ms (Figure 1C). But, aggregation of T-flp53 was much slower, occurring after 7.5 h (Figure 1D). p53tet was highly stable and no aggregation was observed even after incubation at 37°C for 2 days.

T_m changes roughly in a linear fashion with change in free energy of denaturation on mutation but the rate of unfolding changes in an exponential manner with free energy change and consequently, an increase in stability of several kcal mol^{-1} can increase the $t_{1/2}$ of unfolding from several minutes to a few hours (31). All the experiments in the present study were carried out on the framework of the super-stable mutant T-flp53 and p53tet and the total experimental time scale at any point did not exceed 6.5 h at 37°C.

The observed diffusion times of either unbound molecule or the bound complex and their respective molecular weights calculated from the diffusion time are listed in Table 1. Those calculated values of M_w were higher than the expected and arose most likely because the spherical shape assumption in the equations does not hold true, as flp53 is non-globular with intrinsically disordered TAD and unstructured CTD (2).

Determination of dissociation kinetics and equilibrium constants of p53tet

We next measured the dissociation kinetics of p53tet to dimers and monomers. To this end, a working concentration of 0.1 nM of p53tet was achieved by rapid manual dilution of 1 μM of Atto 655-labeled p53tet in the sample dish of the FCS set-up. ACFs were measured for different time intervals immediately following dilution (Figure 2A). Since it was not practically possible to distinguish the different components (bound and unbound) from the analysis of ACF, an average diffusion time was obtained by fitting the ACFs to single diffusion component model. We observed a change in average diffusion time from 183 ± 4 to 115 ± 3 μs and this change was statistically significant ($*P < 0.1$). Dissociation kinetics was obtained by plotting the diffusion time against the different time intervals of incubation. Since dissociation of p53tet involves two equilibria, tetramer-dimer (T ↔ D) and dimer-monomer (D ↔ M), the kinetic plot was fitted using a double-exponential model (Figure 2B). The fit results gave $t_{1/2}$ of 2.5 min and 13 min for the two processes at 37°C. We hypothesized that the dissociation of tetramer to dimer was rapid, with a half-life of 2.5 min, while dimer to monomer transition occurred more slowly. (A slow step followed by a fast one would give a double exponential with only a small amplitude for the fast phase, but we found less than a factor of two difference between the phases). To check this, we determined the dissociation kinetics of a dimeric mutant (L344A) that dimerizes but has impaired tetramerization (32). The $t_{1/2}$ of 16 min for dimer→monomer is consistent with the dissociation of p53tet dimer to monomer occurring more slowly than does tetramer to dimers.

We then determined the dissociation constant (K_d) of p53tet to dimers and monomers. ACFs were measured for the pre-incubated samples of Atto 655-labeled p53tet (0.1 nM) with increasing amounts of unlabeled p53tet (up to 2 μM) (Figure 2C). A single-component fit was used to deduce the average diffusion time. Binding curves obtained by plotting the average diffusion time versus p53 concentration revealed a characteristic two-step equilibrium (Figure 2D). Fitting of the titration curve for the T ↔ D and D ↔ M equilibrium yielded K_ds of 150 nM and 1 nM respectively. The two equilibria were well separated in time by three diffusing species with a lag time of 113, 145 and 186 μs, corresponding to monomers, dimers and tetramers respectively (see Table 1 for calculated M_w). Control experiments using Atto 655-labeled L344P p53tet mutant [monomeric mutant that has impaired oligomerization (32)] showed no change in diffusion time, confirming that the increase in diffusion time is due to the progressive formation of tetramer (Figure 2D).

We choose to perform experiments at 20 and 37°C, as published experimental results are available for comparison for the former while the latter is at physiological temperature and so data recorded under these conditions are more relevant. The dissociation kinetics and equilibrium constants were summarized in Table 2.

Table 1. Diffusion times and molecular weight of various protein samples at 37°C

Sample	Diffusion time (μs)	M_{ws} (kDa) From FCS	calculated M_w (KDa)
Free dye	56 ± 2	–	0.6
p53tet (monomer)	114 ± 3	5.0	4.5
p53tet (tetramer)	183 ± 4	21.0	18
T-flp53 (monomer)	243 ± 5	50	44
T-flp53 (tetramer)	390 ± 3	204	175
P21 RE	180 ± 6	20	16
P21 RE+ T-flp53	396 ± 7	212	191

M_w of Atto 655 dye was used as a reference. M_w of different samples, assuming spherical shape, were calculated using the formula $M_{wf}/M_{ws} = \sim (\tau_f/\tau_s)^3$, where M_{wf} and τ_f, M_{ws} and τ_s, are molecular weight and diffusion time of Atto 655 free dye and samples, respectively. Experiments were carried out in triplicates and error represent ± 1SD.

Determination of dissociation kinetics and equilibrium constants of T-flp53

We next investigated the kinetics and equilibria of oligomerization of flp53, using identical procedures to those described for p53tet. The dissociation kinetics of flp53 was followed by measuring the average diffusion time at

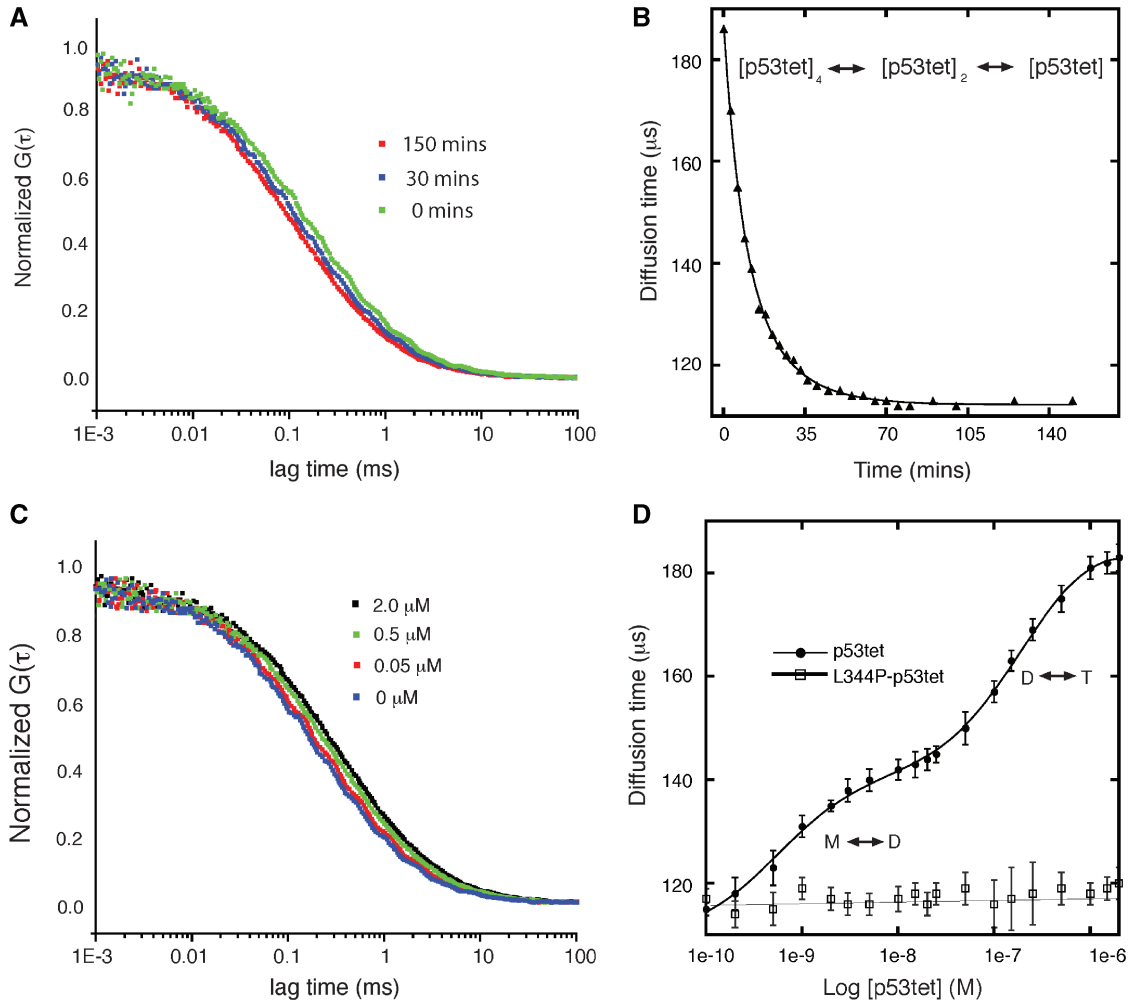

Figure 2. Dissociation kinetics and equilibrium constants of p53tet oligomerization measured using FCS. (**A**) Normalized ACFs following the dissociation of p53tet at 0, 30 and 150 min. (**B**) Plot of the dissociation kinetics of p53tet with 2-exponential data fit. (**C**) Binding of 0.1 nM Atto 655 labeled p53tet to unlabeled p53tet. ACFs measured at unlabeled p53tet concentrations of 0, 0.05, 0.5 and 2 μM is shown. (**D**) Binding curve showing the M ↔ D and D ↔ T equilibrium of p53tet. Log scale is used along X-axis for clarity. The first data point was measured with sample containing only 0.1 nM of labeled p53tet.

Table 2. Equilibrium and half-life of dissociation measured for p53tet and T-flp53

Equilibrium	p53tet				T-flp53			
	$t_{1/2}$ (min)		K_d (nM)		$t_{1/2}$ (min)		K_d (nM)	
	20°C	37°C	20°C	37°C	20°C	37°C	20°C	37°C
T ↔ D	6.5 ± 0.9	2.5 ± 0.4	60 ± 9	150 ± 14	50 ± 7	20 ± 3	20 ± 3	50 ± 7
D ↔ M	55 ± 0.8	13 ± 2	0.5 ± 0.07	1 ± 0.14	250 ± 21	50 ± 7	~0.2[a]	0.55 ± 0.08

T ↔ D represents tetramer to dimer equilibrium and D ↔ M represents dimer to monomer equilibrium. p53tet is isolated tetramerization domain (325–355) and T-flp53 is full-length p53 (1–393) in a super-stable mutant background. Experiments were carried out in buffer containing 25 mM sodium phosphate, 150 mM NaCl, 3 mM DTT, pH 7.2 at 20°C and 37°C. Experiments were carried out in triplicate and ± standard error are presented.

[a]Not quantifiable accurately because of high affinity for dimerization at 20°C, but is <0.25 nM. We estimated the tabulated value from the observed rate constant for dissociation and an estimated rate constant for association (~$2 \times 10^4 s^{-1} M^{-1}$, see Table 3).

regular time intervals (Figure 3A). The dissociation kinetics of flp53 was ~8-fold slower than for p53tet, with $t_{1/2}$ of 20 min and 50 min for the T ↔ D and D ↔ M events at 37°C, respectively (Figure 3B).

We next measured the equilibrium constants for the T ↔ D and D ↔ M equilibria. Atto 655 labeled T-flp53 (0.1 nM) was incubated with increasing concentrations of unlabeled p53 for 5 h at 37°C. ACFs were measured

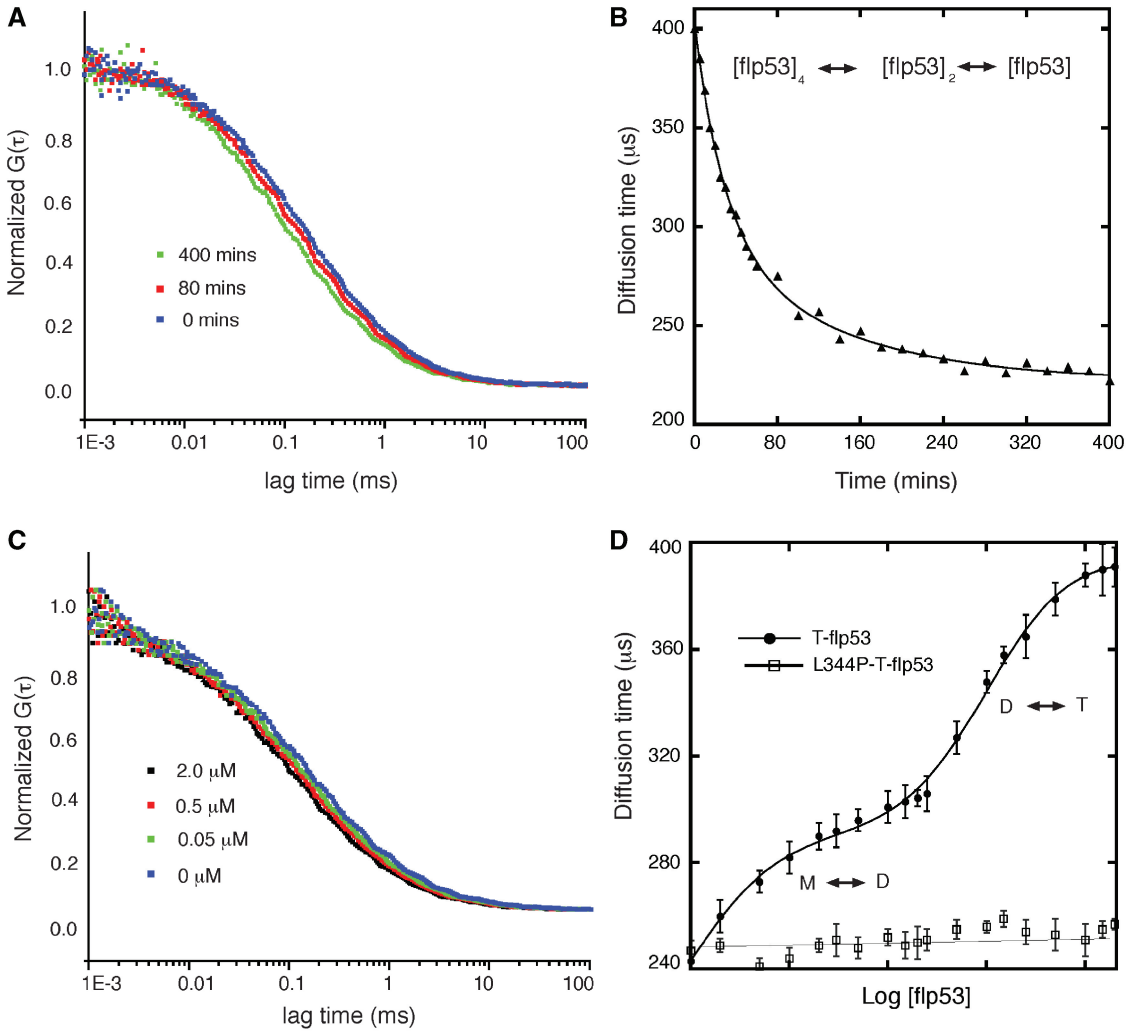

Figure 3. Dissociation kinetics and equilibrium constants of T-flp53 oligomerization measured using FCS. (**A**) Normalized ACFs following the dissociation of T-flp53 at 0, 30 and 150 min. (**B**) Plot of the dissociation kinetics of T-flp53 with 2-exponential fit. (**C**) Binding of 0.1 nM Atto 655 labeled T-flp53 to unlabeled T-flp53. ACFs measured at unlabeled T-flp53 concentrations of 0, 0.05, 0.5 and 2 μM is shown. (**D**) Binding curve showing the M ↔ D and D ↔ T equilibrium of flp53. Log scale is used along X-axis for clarity. The first data point was measured with sample containing only 0.1 nM of labeled flp53.

immediately after incubation (Figure 3C). A progressive change in the diffusion time from 243 ± 6 to 391 ± 3 μs was observed and this change was statistically significant ($*P < 0.1$). No very slowly diffusing species was observed during the measurements, indicating the absence of aggregates. Fitting of the plot derived from average diffusion time of flp53 at various concentrations gave K_ds of 50 nM and 0.55 nM at 37°C for the T ↔ D and D ↔ M equilibria, respectively (Figure 3D). The dissociation constants were ~3-fold lower than those for p53tet. Control experiments using Atto 655-labeled T-flp53-L344P [monomeric mutant that has impaired oligomerization (32)] showed no change in diffusion time upon incubation with varying amounts of unlabeled T-flp53, thus confirming the observed change in diffusion time with Atto 655-labeled T-flp53 was caused by oligomerization (Figure 3D). Table 2 lists the kinetics and equilibrium quantities measured for flp53 and p53tet at 20 and 37°C.

Rate constants for association

We calculated the rate constants for association (k_{ass}) of monomers to dimers and dimers to tetramers from the rate constants for dissociation and the K_ds (Table 3). The k_{ass}s were much smaller than diffusion-controlled limit, indicating a complex energy barrier-limited binding process rather than a diffusion-controlled one.

Influence of DNA on the tetramerization equilibrium of p53

We next investigated how addition of DNA influences the D ↔ T equilibrium. For this purpose, we used Atto 655-labeled p21 response element (26 bp) and Atto 655-labeled bax response element (27 bp) in FCS experiments. p21 RE and bax RE are two of the many p53-target genes that directly mediate cell-cycle arrest and apoptosis respectively (1). p53 binds to p21 and bax response elements with K_ds of ~8 and 184 nM

Table 3. Kinetic rate constants measured for p53tet and T-flp53

Reaction	p53tet				T-flp53			
	k_{ass} ($s^{-1}M^{-1}$)		k_{diss} (s^{-1})		k_{ass} ($s^{-1}M^{-1}$)		k_{diss} (s^{-1})	
	20°C	37°C	20°C	37°C	20°C	37°C	20°C	37°C
T ↔ D	3×10^4	3.1×10^4	1.8×10^{-3}	4.6×10^{-3}	1.2×10^4	1.2×10^4	2.3×10^{-4}	5.8×10^{-4}
D ↔ M	4.2×10^5	8.9×10^5	2.1×10^{-4}	8.9×10^{-4}	–	4.2×10^5	4.6×10^{-5}	2.3×10^{-4}

The rate constants for association, k_{ass}, are calculated from K_d and the rate constant k_{diss} measured from FCS experiments.

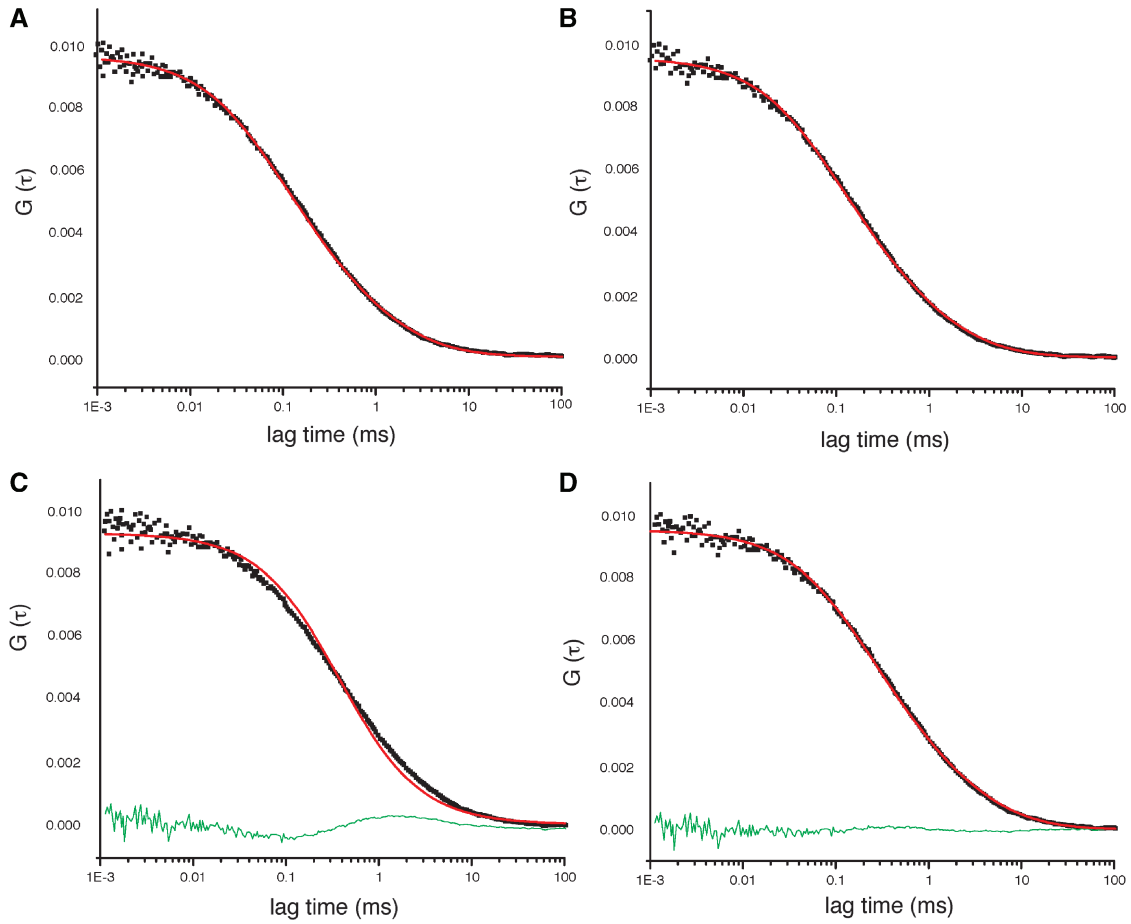

Figure 4. DNA binding experiments of T-flp53 to Atto 655 labeled p21 and bax RE. (**A**) ACF of Atto 655-labeled p21 RE. Fitting to a single diffusion model yielded τ of 180 µs. (**B**) FCS curve of sample containing 10 nM T-flp53 and 5 nM Atto 655 labeled bax RE. No difference in diffusion time as compared to free Atto 655 labeled bax RE was observed. (**C**) Single component fit of the ACF obtained from the sample containing 10 nM of T-flp53 and 5 nM of Atto 655 labeled p21 RE. Residual of the fit is shown in green. (**D**) Two-component fit of the ACF of sample containing 10 nM of T-flp53 and 5 nM of Atto 655 labeled p21 RE (τ = 180 and 396 µs). Residual of the fit is shown in green.

respectively (15). The diffusion times of Atto 655-labeled p21 RE and bax RE were measured to be 180 and 183 µs, respectively (Figure 4A). We measured ACFs for a mixture containing Atto 655-labeled bax (5 nM) and unlabeled T-flp53 (10 nM). At a concentration of 10 nM, p53 is predominantly dimeric as measured earlier. No significant change in diffusion time, compared with free bax RE, was observed for the complex (Figure 4B). Under the same experimental conditions, the influence of p21 on the D ↔ T equilibrium was investigated. ACF was measured upon addition of unlabeled protein, but the fitting of ACF to a single component 2D model yielded a poor fit (Figure 4C). Hence a two-diffusion component model was used keeping the diffusion time of free p21 (180 µs) as a fixed parameter in the fit. The fitting quality improved significantly and yielded a diffusion time of 396 µs for the slowly diffusing component (Figure 4D). Using Atto 655 labeled p21 as reference with τ = 180 µs and M_w = 16 kDa, the apparent M_w of the complex with τ = 396 µs was ~212 kDa (calculated

using the relation $M_{wf}/M_{ws} = \sim (\tau_f/\tau_s)^3$, using Atto 655 dye as reference, see Table 1 for details). This is close to the theoretical molecular weight of $[p53]_4$:[p21 DNA] complex (192 KDa). An apparent K_d of ~7 nM was estimated from the amplitudes of free p21 RE and the bound complex, which is in good agreement with previous results (15). Lack of binding in control experiments using the full-length p53 R273H mutant that has impaired DNA-binding ability (33) confirmed that the formation of $[p53]_4$:[p21 DNA] complex resulted from the sequence-specific DNA binding of p53. The sequence-specific binding of bax RE was not detected because its K_d ~184 nM is too high (15).

DISCUSSION

We investigated the dissociation kinetics and thermodynamic equilibria of tetramer–dimer–monomer transitions of full-length p53 and p53tet using fluorescence correlation spectroscopy. We first measured the lag phase in the kinetics of aggregation (Figure 1) to make sure that our data were collected prior to any artifacts arising from irreversible events.

Analytical ultracentrifugation (AUC) has previously been used to characterize the tetramerization equilibria of p53 (14,16,34). Earlier measurements using absorbance detection, tended to give values of ~100–140 nM for the dissociation constant of the tetramer–dimer equilibrium, and were too insensitive to detect the dimer–monomer stage (35). Use of fluorescence detection gives a K_d of 19.4 ± 8.8 nM for tetramers to dimers and 1.0 ± 0.7 nM for dimers to monomers at 10°C in a similar buffer to ours but containing 10% glycerol (14). The value of 1 nM is at the very limit of detection of current AUC detection because experiments have to be performed at concentrations of reagents around their K_d. We obtained reliable data at 37°C of 50 ± 7 nM for tetramer to dimer and 0.55 ± 0.08 for dimer to monomer (Table 2). At 20°C, the dimer-monomer equilibrium was too low to measure, and was estimated to be <0.25 nM. We can calculate an approximate value to be ~0.2 nM from the ratio of the rate constant for dissociation of the dimer to that estimated by comparison for the association of full-length tetramers at 20°C (see note to Table 2).

The rate constants for association of dimers to tetramers and monomers to dimers were calculated from the measured rate and equilibrium constants for dissociation (Table 3). The rate constant for the association of p53tet at 25°C was previously measured from protein folding studies under somewhat different conditions to be $3.1 \times 10^5\,s^{-1}M^{-1}$, and the dissociation rate constant for p53tet tetramer $3.7 \times 10^{-3}\ s^{-1}$ (13), which are in reasonable agreement with values in Table 3 ($4.2 \times 10^5\ s^{-1}$ and $1.8 \times 10^{-3}\,s^{-1}$, respectively). The rate constants for the association of p53tet are 2- to 3-fold higher than for full-length p53. A major contributory factor is the slower rate of diffusion of the large molecules (Table 1), since the target size of the association region is the same for both proteins.

The self-association of full-length p53 is stronger than that for p53tet, by a factor of 3 for dimers to tetramers, and a factor of 2 for monomers to dimers (Table 2). The major reason for tighter binding in both cases is slower dissociation constants, which will reflect a slower diffusion apart, which balances the slower diffusion together, combined with some known weak CD:CD interactions(2,35).

This study demonstrates the power of FCS as a quantitative protein binding assay for tight binders due to its single-molecule sensitivity (detection limit being low pM). The slow dissociation kinetics competing with spontaneous denaturation of WT p53 has direct implications in the dominant negative effect exerted by hetero-oligomerization with mutant p53.

Biological implications

Although the measurements of dissociation constants in the present study were *in vitro*, they were measured at physiological temperature, pH and ionic strength, and so do have some bearing on *in vivo*, especially as the dissociation constants for monomer–dimer and dimer–tetramer differ by 100-fold. p53 protein levels are normally low in unstressed cells due to rapid turnover, but in response to various stress stimuli, p53 is stabilized leading to higher levels and activated. The actual cellular concentration of p53 has not been measured experimentally to date, although a basal level of 1–10 nM has been suggested (34). If this number holds true, then p53 exists predominantly as dimers in the cellular pool. However, due to the high affinity of p53 dimer to p21 response element (which is much higher than the inherent dissociation constant of p53 tetramer), a major fraction of p53 is expected to be bound to p21 response element (or any promoters of similar affinity). Hence, upon stress, only an activation signal (such as posttranslational modifications) is necessary to begin transactivation. However, for transactivation of promoters such as bax, enough p53 has to be accumulated before binding to the response element. Consequently, following stress stimuli, p53 levels must increase for transactivation of bax to occur. In support of this hypothesis, using CHIP experiments it has been shown that p53 is bound to p21 promoter in unstressed cells. Further induction of p21 occurs rapidly upon stress. On the other hand, little p53 is bound to bax promoter in unstressed cells and induction of bax occurs with delayed kinetics (36).

But, superimposed upon the equilibria of unligated p53 is a complex regulation of the oligomeric state of p53 by partner proteins. p53-interacting proteins such as 14-3-3, Ref-1, BCCIP, c-Abl, provides another layer in the functional activation of p53 by facilitating p53 tetramerization (16,37). Furthermore, cellular function of p53 is tightly regulated at the level of p53 transcription and protein stability. This is often achieved by posttranslational modifications and protein–protein interactions, which lead to either increased stability or degradation (1,38). For instance, the S100 family of proteins (S100A4 and S100B) binds to monomeric, dimeric or tetrameric forms of p53 and in turn regulate its activity (39,40). Binding of

S100 to monomeric or dimeric forms is proposed to deregulate the activity of p53 (39). However, in order to disrupt tetramerization, S100B must compete for the dimer-tetramer equilibrium. The affinity of S100B to tetramerization domain of p53 (~50 μM) is much weaker than the inherent p53 tetramerization, as measured here and, therefore, high levels of S100B is necessary to disrupt tetramerization and impair p53 function (39). In support of this idea, it has been shown that very high levels of S100B, as observed in some tumors, prevent p53 tetramerization and consequently inhibit its activity (41).

ACKNOWLEDGEMENTS

The authors thank Drs H. Neuweiler, J.L. Kaar and C.M. Johnson for their technical help and fruitful discussions. S.R is supported by a fellowship from Medical Research Council.

FUNDING

Fellowship from Medical Research Council (to S.R.). Funding for open access charge: Medical Research Council (MRC).

Conflict of interest statement. None declared.

REFERENCES

1. Vousden,K.H. and Prives,C. (2009) Blinded by the light: the growing complexity of p53. *Cell*, **137**, 413–431.
2. Tidow,H., Melero,R., Mylonas,E., Freund,S.M., Grossmann,J.G., Carazo,J.M., Svergun,D.I., Valle,M. and Fersht,A.R. (2007) Quaternary structures of tumor suppressor p53 and a specific p53 DNA complex. *Proc. Natl Acad. Sci. USA*, **104**, 12324–12329.
3. Petitjean,A., Mathe,E., Kato,S., Ishioka,C., Tavtigian,S.V., Hainaut,P. and Olivier,M. (2007) Impact of mutant p53 functional properties on TP53 mutation patterns and tumor phenotype: lessons from recent developments in the IARC TP53 database. *Hum. Mutat.*, **28**, 622–629.
4. Nicholls,C.D., McLure,K.G., Shields,M.A. and Lee,P.W. (2002) Biogenesis of p53 involves cotranslational dimerization of monomers and posttranslational dimerization of dimers. Implications on the dominant negative effect. *J. Biol. Chem.*, **277**, 12937–12945.
5. Varley,J.M., McGown,G., Thorncroft,M., Cochrane,S., Morrison,P., Woll,P., Kelsey,A.M., Mitchell,E.L., Boyle,J., Birch,J.M. *et al.* (1996) A previously undescribed mutation within the tetramerisation domain of TP53 in a family with Li-Fraumeni syndrome. *Oncogene*, **12**, 2437–2442.
6. Weinberg,R.L., Veprintsev,D.B. and Fersht,A.R. (2004) Cooperative binding of tetrameric p53 to DNA. *J. Mol. Biol.*, **341**, 1145–1159.
7. McLure,K.G. and Lee,P.W. (1998) How p53 binds DNA as a tetramer. *EMBO J.*, **17**, 3342–3350.
8. Chene,P. and Jahnke,W. (2002) Oligomerization of p53 upon cooperative DNA binding: towards a structural understanding of p53 function. *Angew Chem. Int. Ed. Engl*, **41**, 1702–1704.
9. Stenger,J.E., Tegtmeyer,P., Mayr,G.A., Reed,M., Wang,Y., Wang,P., Hough,P.V. and Mastrangelo,I.A. (1994) p53 oligomerization and DNA looping are linked with transcriptional activation. *EMBO J.*, **13**, 6011–6020.
10. Itahana,Y., Ke,H. and Zhang,Y. (2009) p53 Oligomerization is essential for its C-terminal lysine acetylation. *J. Biol. Chem.*, **284**, 5158–5164.
11. Maki,C.G. (1999) Oligomerization is required for p53 to be efficiently ubiquitinated by MDM2. *J. Biol. Chem.*, **274**, 16531–16535.
12. Shieh,S.Y., Taya,Y. and Prives,C. (1999) DNA damage-inducible phosphorylation of p53 at N-terminal sites including a novel site, Ser20, requires tetramerization. *EMBO J.*, **18**, 1815–1823.
13. Mateu,M.G., Sanchez Del Pino,M.M. and Fersht,A.R. (1999) Mechanism of folding and assembly of a small tetrameric protein domain from tumor suppressor p53. *Nat. Struct. Biol.*, **6**, 191–198.
14. Brandt,T., Petrovich,M., Joerger,A.C. and Veprintsev,D.B. (2009) Conservation of DNA-binding specificity and oligomerisation properties within the p53 family. *BMC Genomics*, **10**, 628.
15. Natan,E., Hirschberg,D., Morgner,N., Robinson,C.V. and Fersht,A.R. (2009) Ultraslow oligomerization equilibria of p53 and its implications. *Proc. Natl Acad. Sci. USA*, **106**, 14327–14332.
16. Rajagopalan,S., Jaulent,A.M., Wells,M., Veprintsev,D.B. and Fersht,A.R. (2008) 14-3-3 activation of DNA binding of p53 by enhancing its association into tetramers. *Nucleic Acids Res.*, **36**, 5983–5991.
17. Rajagopalan,S., Andreeva,A., Teufel,D.P., Freund,S.M. and Fersht,A.R. (2009) Interaction between the transactivation domain of p53 and PC4 exemplifies acidic activation domains as single-stranded DNA mimics. *J. Biol. Chem.*, **284**, 21728–21737.
18. Huang,F., Rajagopalan,S., Settanni,G., Marsh,R.J., Armoogum,D.A., Nicolaou,N., Bain,A.J., Lerner,E., Haas,E., Ying,L. *et al.* (2009) Multiple conformations of full-length p53 detected with single-molecule fluorescence resonance energy transfer. *Proc. Natl Acad. Sci. USA*, **106**, 20758–20763.
19. Neuweiler,H., Johnson,C.M. and Fersht,A.R. (2009) Direct observation of ultrafast folding and denatured state dynamics in single protein molecules. *Proc. Natl Acad. Sci. USA*, **106**, 18569–18574.
20. Meseth,U., Wohland,T., Rigler,R. and Vogel,H. (1999) Resolution of fluorescence correlation measurements. *Biophys. J.*, **76**, 1619–1631.
21. Muller,J.D., Chen,Y. and Gratton,E. (2003) Fluorescence correlation spectroscopy. *Methods Enzymol.*, **361**, 69–92.
22. Schwille,P. (2001) Fluorescence correlation spectroscopy and its potential for intracellular applications. *Cell. Biochem. Biophys.*, **34**, 383–408.
23. Berland,K.M. (2004) Fluorescence correlation spectroscopy: a new tool for quantification of molecular interactions. *Methods Mol. Biol.*, **261**, 383–398.
24. Rigler,R. (1995) Fluorescence correlations, single molecule detection and large number screening. Applications in biotechnology. *J. Biotechnol.*, **41**, 177–186.
25. Doose,S., Neuweiler,H., Barsch,H. and Sauer,M. (2007) Probing polyproline structure and dynamics by photoinduced electron transfer provides evidence for deviations from a regular polyproline type II helix. *Proc. Natl Acad. Sci. USA*, **104**, 17400–17405.
26. Rauer,B., Neumann,E., Widengren,J. and Rigler,R. (1996) Fluorescence correlation spectrometry of the interaction kinetics of tetramethylrhodamin alpha-bungarotoxin with Torpedo californica acetylcholine receptor. *Biophys. Chem.*, **58**, 3–12.
27. Friedler,A., Veprintsev,D.B., Hansson,L.O. and Fersht,A.R. (2003) Kinetic instability of p53 core domain mutants: implications for rescue by small molecules. *J. Biol. Chem.*, **278**, 24108–24112.
28. Nikolova,P.V., Henckel,J., Lane,D.P. and Fersht,A.R. (1998) Semirational design of active tumor suppressor p53 DNA binding domain with enhanced stability. *Proc. Natl Acad. Sci. USA*, **95**, 14675–14680.
29. Joerger,A.C., Ang,H.C. and Fersht,A.R. (2006) Structural basis for understanding oncogenic p53 mutations and designing rescue drugs. *Proc. Natl Acad. Sci. USA*, **103**, 15056–15061.
30. Ruttinger,S., Buschmann,V., Kramer,B., Erdmann,R., Macdonald,R. and Koberling,F. (2008) Comparison and accuracy of methods to determine the confocal volume for quantitative fluorescence correlation spectroscopy. *J. Microsc.*, **232**, 343–352.
31. Godoy-Ruiz,R., Ariza,F., Rodriguez-Larrea,D., Perez-Jimenez,R., Ibarra-Molero,B. and Sanchez-Ruiz,J.M. (2006) Natural selection

for kinetic stability is a likely origin of correlations between mutational effects on protein energetics and frequencies of amino acid occurrences in sequence alignments. *J. Mol. Biol.*, **362**, 966–978.
32. Davison,T.S., Nie,X., Ma,W., Lin,Y., Kay,C., Benchimol,S. and Arrowsmith,C.H. (2001) Structure and functionality of a designed p53 dimer. *J. Mol. Biol.*, **307**, 605–617.
33. Ang,H.C., Joerger,A.C., Mayer,S. and Fersht,A.R. (2006) Effects of common cancer mutations on stability and DNA binding of full-length p53 compared with isolated core domains. *J. Biol. Chem.*, **281**, 21934–21941.
34. Sakaguchi,K., Sakamoto,H., Lewis,M.S., Anderson,C.W., Erickson,J.W., Appella,E. and Xie,D. (1997) Phosphorylation of serine 392 stabilizes the tetramer formation of tumor suppressor protein p53. *Biochemistry*, **36**, 10117–10124.
35. Veprintsev,D.B., Freund,S.M., Andreeva,A., Rutledge,S.E., Tidow,H., Canadillas,J.M., Blair,C.M. and Fersht,A.R. (2006) Core domain interactions in full-length p53 in solution. *Proc. Natl Acad. Sci. USA*, **103**, 2115–2119.
36. Kaeser,M.D. and Iggo,R.D. (2002) Chromatin immunoprecipitation analysis fails to support the latency model for regulation of p53 DNA binding activity in vivo. *Proc. Natl Acad. Sci. USA*, **99**, 95–100.
37. Rajagopalan,S., Sade,R.S., Townsley,F.M. and Fersht,A.R. (2010) Mechanistic differences in the transcriptional activation of p53 by 14-3-3 isoforms. *Nucleic Acids Res.*, **38**, 893–906.
38. Kruse,J.P. and Gu,W. (2009) Modes of p53 regulation. *Cell*, **137**, 609–622.
39. Fernandez-Fernandez,M.R., Veprintsev,D.B. and Fersht,A.R. (2005) Proteins of the S100 family regulate the oligomerization of p53 tumor suppressor. *Proc. Natl Acad. Sci. USA*, **102**, 4735–4740.
40. van Dieck,J., Fernandez-Fernandez,M.R., Veprintsev,D.B. and Fersht,A.R. (2009) Modulation of the oligomerization state of p53 by differential binding of proteins of the S100 family to p53 monomers and tetramers. *J. Biol. Chem.*, **284**, 13804–13811.
41. Lin,J., Blake,M., Tang,C., Zimmer,D., Rustandi,R.R., Weber,D.J. and Carrier,F. (2001) Inhibition of p53 transcriptional activity by the S100B calcium-binding protein. *J. Biol. Chem.*, **276**, 35037–35041.